

Article

Simple Synthesis and Characterization of Cobalt Ferrite Nanoparticles for the Successful Adsorption of Indigo Carmine Dye from Aqueous Media

Asma S. Al-Wasidi ¹ and Ehab A. Abdelrahman ^{2,3,*} 

¹ Department of Chemistry, College of Science, Princess Nourah bint Abdulrahman University, Riyadh 11671, Saudi Arabia

² Department of Chemistry, College of Science, Imam Mohammad Ibn Saud Islamic University (IMSIU), Riyadh 11623, Saudi Arabia

³ Chemistry Department, Faculty of Science, Benha University, Benha 13518, Egypt

* Correspondence: eaaahmed@imamu.edu.sa

Abstract: Indigo carmine dye falls into the category of toxic chemicals, potentially leading to irritation and allergic reactions in certain individuals. Thus, this study employed the Pechini sol–gel strategy to easily produce CoFe_2O_4 nanoparticles, which serve as an effective adsorbent for the disposal of indigo carmine dye from aqueous solutions. The maximum adsorption capacity of CoFe_2O_4 for indigo carmine dye was determined to be 421.94 mg/g. The synthesized CoFe_2O_4 nanoparticles exhibited an average crystallite size of 18.75 nm. SEM analysis revealed that these nanoparticles were nearly spherical, with an average grain size of 198.32 nm. Additionally, TEM analysis indicated a fully agglomerated spherical morphology for the CoFe_2O_4 sample, with an average diameter of 15.37 nm. The EDS spectrum confirmed that the synthesized CoFe_2O_4 nanoparticles consisted of Co, Fe, and O elements, with respective weight percentages of 17.82%, 49.46%, and 32.72%. The removal of indigo carmine dye by the synthesized CoFe_2O_4 is spontaneous, chemical, exothermic, closely fitting the pseudo-second-order kinetic model, and demonstrating a strong concordance with the Langmuir equilibrium isotherm.

Keywords: adsorption; indigo carmine dye; CoFe_2O_4 nanoparticles; characterization



Citation: Al-Wasidi, A.S.; Abdelrahman, E.A. Simple Synthesis and Characterization of Cobalt Ferrite Nanoparticles for the Successful Adsorption of Indigo Carmine Dye from Aqueous Media. *Inorganics* **2023**, *11*, 453. <https://doi.org/10.3390/inorganics11120453>

Academic Editor: Carlos Martínez-Boubeta

Received: 28 October 2023

Revised: 15 November 2023

Accepted: 17 November 2023

Published: 24 November 2023



Copyright: © 2023 by the authors. Licensee MDPI, Basel, Switzerland. This article is an open access article distributed under the terms and conditions of the Creative Commons Attribution (CC BY) license (<https://creativecommons.org/licenses/by/4.0/>).

1. Introduction

Water sources, encompassing seas, clouds, rivers (in the form of ice, snow, and rain), and the underground, serve as reservoirs of pure water. Inherently pure, water is instrumental in extracting, purifying, and solubilizing various substances. Its designation as the universal solvent stems from its high polarity and omnipresence in all facets of life. The physical properties of water may undergo changes either through the influence of nonpolluting agents originating from its source, such as rocks, clay, sand, and algal blooms resulting from water stagnation, or due to deleterious pollutants introduced by human activities [1–4]. Consequently, the quest for obtaining pure water has evolved into a formidable challenge, necessitating the protection of water sources. Moreover, climate change-induced droughts and the proliferation of industrial installations pose escalating threats to water sources. In the pre-industrial revolution era, natural dyes derived from sources like insects, flowering plants, vegetables, and roots were prevalent. However, the surging demand for dyes has led industries to rely more on synthetic alternatives, known for their rapid coloration process, increased solubility, easy absorbability, and versatility compared to their natural counterparts. Among the industries, textiles stand out as significant water consumers, releasing substantial quantities of synthetic dyes into wastewater, thereby contaminating water resources and land. Other sectors, such as printing, cosmetics, food packaging, pharmaceuticals, and processing, also contribute to dye

pollution, but their impact is comparatively lesser than that of the textile industry [5–8]. Over 15% of the dyes employed in textiles are released into the environment without binding to the fibers, often mingling with other organic and inorganic additives designed to enhance dye adsorption on fabrics. Consequently, these chemicals typically find their way into soils and surfaces [9–12]. The textile industry stands as a significant contributor to wastewater containing organic dyes [13–15]. Among these dyes, indigo carmine, also referred to as 5,5'-indigodisulfonic acid sodium salt, holds particular importance due to its widespread utilization in various industries, including textiles, as well as paper, plastic, leather, food, cosmetics, and printing [16,17]. These organic dyes are prevalent water contaminants and pose potential threats to both human health and ecosystems, given their mutagenic and carcinogenic characteristics [2,18]. Hence, a pressing requirement exists for the elimination of these organic dyes from wastewater discharges. Various methods have been explored to address water bodies contaminated with organic dyes, encompassing processes like photocatalysis [19–21], chemical coagulation and precipitation [22], biodegradation [23], membrane filtration [24], electrochemistry [25], and adsorption [21,26–28]. Of these methods, adsorption stands out as one of the most effective processes and is commonly employed. This is because alternative techniques often necessitate a significant amount of chemicals and/or substantial energy input, making them costlier [29–32]. Numerous materials have been explored for the elimination of indigo carmine from solutions. These materials encompass activated carbon [33,34], natural substances [35,36], polyacrylonitrile/Fe₃O₄/3-mercaptopropionic acid composites [37], montmorillonite [38], chitosan aerogels [39], and carbon nanotubes [40]. However, the use of certain materials is restricted due to their high cost, limited adsorption capacity, challenges associated with their disposal and reusability, and the ongoing difficulty of separating these adsorbents from aqueous solutions. Metal ferrite nanoparticles, including zinc ferrite, manganese ferrite, and magnesium ferrite, have gained considerable attention for their effectiveness as adsorbents in the removal of dyes, heavy metals, and various waterborne contaminants from aqueous environments [41–44]. These metal ferrite adsorbents are preferred due to their small crystal size, large surface area, and significant pore volume, allowing for faster adsorption and higher adsorption capacity compared to conventional adsorbents. Moreover, metal ferrite adsorbents with magnetic properties offer an additional advantage, making their retrieval from water more convenient. This feature facilitates easy recycling and reduces operational costs [45–48]. This research delves into the adsorption capabilities of magnetic cobalt ferrite nanoparticles for eliminating indigo carmine dye from aqueous solutions. The cobalt ferrite nanoparticles were readily manufactured through the Pechini sol-gel technique and underwent thorough characterization to evaluate their crystalline structure, morphology, and the active chemical bonds present on their surface. A comprehensive examination was carried out to understand how various experimental variables, including solution pH, reaction time, reaction temperature, and initial dye concentration, influenced the removal efficiency of indigo carmine dye. Moreover, applied kinetic and equilibrium modelling were studied to gain insights into the adsorption process. Additionally, a thermodynamic investigation was conducted to grasp the influence of reaction temperature on the adsorption of indigo carmine dye onto cobalt ferrite nanoparticles. Lastly, this research delved into aspects of regeneration and reusability. Hence, the novelty of this work lies in the innovative approach of synthesizing cobalt ferrite nanoparticles utilizing the Pechini sol-gel method while incorporating tartaric acid as a chelating agent and 1,2-propanediol as a cross-linker. This specific combination of synthesis parameters has not been previously reported, marking the first instance of employing these precise conditions for the production of cobalt ferrite nanoparticles. The use of tartaric acid as a chelating agent and 1,2-propanediol as a cross-linker in conjunction with the Pechini sol-gel method introduces a novel methodology that may yield distinct and advantageous characteristics in the resulting nanoparticles, offering potential advancements in the field of water treatment due to the low crystal size and high adsorption capacity of the sample towards indigo carmine dye.

2. Experimental

2.1. Materials

Cobalt(II) nitrate hexahydrate ($\text{Co}(\text{NO}_3)_2 \cdot 6\text{H}_2\text{O}$), tartaric acid ($\text{C}_4\text{H}_6\text{O}_6$), iron(III) nitrate nonahydrate ($\text{Fe}(\text{NO}_3)_3 \cdot 9\text{H}_2\text{O}$), hydrochloric acid (HCl), potassium nitrate (KNO_3), sodium hydroxide (NaOH), 1,2-propanediol ($\text{C}_3\text{H}_8\text{O}_2$), and indigo carmine dye ($\text{C}_{16}\text{H}_8\text{N}_2\text{Na}_2\text{O}_8\text{S}_2$) were purchased from Sigma-Aldrich (St. Louis, MO, USA).

2.2. Synthesis of CoFe_2O_4 Nanoparticles

The cobalt(II) solution was freshly produced by dissolving 4.50 g of cobalt(II) nitrate hexahydrate in 90 mL of deionized water. Moreover, the iron(III) solution was freshly produced by carefully dissolving 12.49 g of iron(III) nitrate nonahydrate in 110 mL of deionized water. Subsequently, the cobalt(II) solution was slowly added drop-by-drop to the iron(III) solution, and the resulting mixture was continuously stirred for 10 min using a magnetic stirrer at a temperature of 25 °C. Additionally, the tartaric acid solution (9.28 g of tartaric acid dissolved in 110 mL of deionized water) was added dropwise to work as a chelating agent; then, the subsequent mixture was stirred continually for 10 min with a magnetic stirrer at 130 °C. Following that, 10 mL of 1,2-propanediol was added drop-by-drop as a cross-linker, and the resulting mixture was gently stirred continually through a magnetic stirrer at 130 °C so that complete evaporation occurred. The resultant solid product endured a calcination treatment at 650 °C for 3 h. Following the calcination process, a sample was delicately crushed with a mortar and pestle to obtain cobalt ferrite nanoparticles in powdered form.

2.3. Characterization

X-ray diffraction (XRD) data of CoFe_2O_4 nanoparticles was gathered using a Bruker D8 Discover X-ray Diffractometer equipped with Cu K_α radiation and a Ni filter, operating at a scanning speed of 8 degrees/minute within the 2θ range of 20–80° ($\lambda = 0.15$ nm, 40 mA, 40 kV, and a step size of 0.02°). Micrographs of CoFe_2O_4 nanoparticles obtained through scanning electron microscopy (SEM) were examined using an FEG250-FEI instrument (Hillsboro, OR, USA), which was operated at 25.0 kV. The elemental composition of the CoFe_2O_4 nanoparticles was examined through energy-dispersive X-ray analysis (EDS) (Hillsboro, OR, USA). The morphology and particle size of the CoFe_2O_4 nanoparticles were assessed using transmission electron microscopy (TEM) on a Thermo Fisher Scientific Talos F200iS instrument (Hillsboro, OR, USA), operated at 200 kV. Fourier-transform infrared spectroscopy (FT-IR) analysis of the CoFe_2O_4 nanoparticles was conducted using KBr wafers on a PerkinElmer spectrometer (Waltham, MA, USA).

2.4. Adsorption of Indigo Carmine Dye from Aqueous Solutions

The effect of solution pH was studied as the following: 0.06 g of CoFe_2O_4 nanoparticles were individually introduced into different batches containing 120 mL solutions containing indigo carmine dye at a concentration of 240 mg/L. Subsequently, the pH of each was fixed at a final pH ranging between 2 and 10, and the mixture was agitated for 240 min using a magnetic stirrer operating at 600 rpm. Further investigations were carried out to examine the influence of adsorption time (ranging from 10 to 140 min) at pH 2, as described and clearly shown in Table 1. Additionally, experiments were conducted to assess the impact of adsorption temperature (ranging from 298 to 328 K) at pH 2 and a fixed duration of 90 min. Furthermore, tests were performed to assess the effect of the initial indigo carmine concentrations (ranging from 40 to 280 mg/L) at pH 2, 298 K, and 90 min. Upon the completion of the adsorption process, an external magnetic field was used to separate the CoFe_2O_4 adsorbent from the solution containing indigo carmine dye. The supernatant was subsequently analyzed to determine any of the remaining dye concentration, with measurements conducted at the maximum absorption wavelength of indigo carmine dye (i.e., 610 nm) using an 1800 series UV–Vis spectrophotometer (Shimadzu, Kyoto, Japan).

Table 1. Practical conditions for removing indigo carmine dye by CoFe₂O₄ nanoparticles.

Effect	Concentration of Dye (mg/L)	Volume of Dye (mL)	Amount of Adsorbent (g)	pH	Time (min)	Temperature (K)
pH	240	120	0.06	2–10	240	298
Time	240	120	0.06	2	10–140	298
Temperature (298–328 K)	240	120	0.06	2	90	298–328
Concentration (40–280 mg/L)	40–280	120	0.06	2	90	298

The elimination percentage of the indigo carmine dye (% R) and the uptake capacity of the CoFe₂O₄ adsorbent (Q, mg/g) were estimated employing Equations (1) and (2), respectively [5,6,26,47].

$$\% R = \frac{C_o - C_e}{C_o} \times 100 \quad (1)$$

$$Q = (C_o - C_e) \times \frac{V}{M} \quad (2)$$

C_o indicates the initial concentration of the indigo carmine dye (mg/L), whereas C_e indicates the equilibrium concentration of the indigo carmine dye (mg/L). The symbol M indicates the dry mass of the CoFe₂O₄ adsorbent (g) whereas V indicates the volume of the indigo carmine dye solution (L).

The CoFe₂O₄ adsorbent's point of zero charge (pH_{PZC}) was ascertained using the salt addition method [48]. A set of 60 mL beakers was prepared, each containing 30 mL of a 0.02 M KNO₃ solution, covering an initial pH (pH_i) range from 2.5 to 11.5. The pH of these samples was adjusted using either 0.1 M NaOH and/or 0.1 M HCl. Subsequently, 0.04 g of CoFe₂O₄ adsorbent was added to each beaker. The solutions were thoroughly mixed and stirred for a duration of 5 h. Following the separation of the solutions, the final pH (pH_f) of the filtrate was measured. The pH_{PZC} was determined by plotting the pH_f against the pH_i, and it was identified as the pH_f value at which a distinct plateau was seen.

3. Results and Discussion

3.1. Synthesis and Characterization of CoFe₂O₄ Nanoparticles

The synthesis of CoFe₂O₄ nanoparticles was achieved using the Pechini sol–gel technique, as outlined in Scheme 1. Initially, the cobalt tartrate/1,2-propanediol network was created through the reaction of Co(NO₃)₂·6H₂O with tartaric acid and 1,2-propanediol. Simultaneously, the ferric tartrate/1,2-propanediol network was formed by reacting Fe(NO₃)₃·9H₂O with tartaric acid and 1,2-propanediol. Following this step, the mixture was subjected to heating at 120 °C until it reached dryness. Subsequently, the resulting powder was subjected to calcination at 650 °C for a duration of 3 h to yield CoFe₂O₄ nanoparticles. Figure 1 illustrates the thermal gravimetric analysis of the produced powder before the calcination process. The sample displayed a decomposition pattern with two steps. The first step, which is located in a range from 25 to 220 °C, can be attributed to the loss of adsorbed water molecules with a weight loss of 13%. The second step, which is located in a range from 220 to 650 °C, can be attributed to the loss of organic moiety with a weight loss of 62%. It is evident that 650 °C was the optimal temperature for the formation of CoFe₂O₄ nanoparticles, where there was no weight loss after 650 °C.

In Figure 2, the XRD pattern of the cobalt ferrite nanoparticles is presented. The diffraction peaks observed in the pattern can be entirely attributed to the cubic spinel phase of cobalt ferrite (CoFe₂O₄, JCPDS No. 22-1086) without any presence of impurities [49]. The average crystal size of the particles was determined to be 18.75 nm using the Debye–Scherrer equation. The peaks found at the 2θ values of 30.07°, 35.34°, 36.99°, 43.05°, 53.37°, 56.91°, 62.48°, 70.92°, and 73.75° were caused by reflections from different Miller planes of

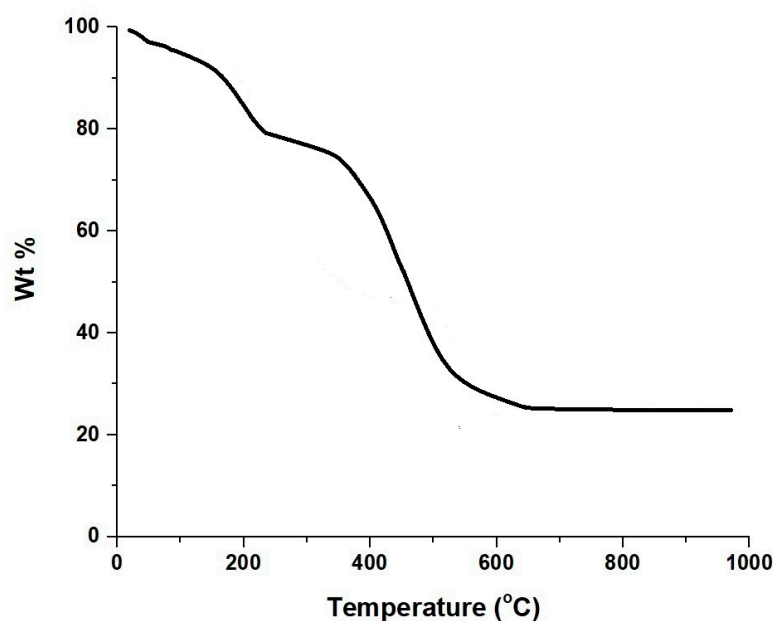


Figure 1. Thermal gravimetric analysis of the produced material prior to the calcination operation.

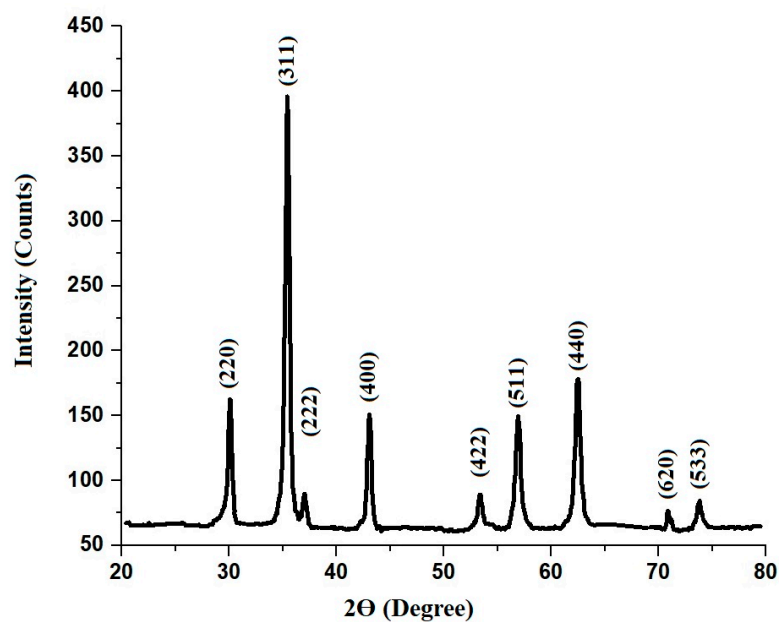


Figure 2. X-ray diffraction analysis of CoFe_2O_4 nanoparticles.

A Fourier-transform infrared spectroscopy (FTIR) analysis was conducted on the synthesized CoFe_2O_4 nanoparticles to examine their functional groups, as depicted in Figure 3. The band at 450 cm^{-1} is ascribed to the stretching vibration of Co-O , while the band at 577 cm^{-1} is ascribed to the stretching vibration of Fe-O . Additionally, the bands at 1635 and 3450 cm^{-1} are ascribed to the bending and stretching vibrations of OH , respectively [49].

The morphology and grain size of the CoFe_2O_4 sample were examined using a scanning electron microscope (SEM), as illustrated in Figure 4A. It is evident from the images that the CoFe_2O_4 nanoparticles exhibited a nearly spherical shape with an average grain size of 198.32 nm . Besides that, the morphology of the synthesized CoFe_2O_4 nanoparticles was also investigated through transmission electron microscope (TEM) analysis, as presented in Figure 4B. The CoFe_2O_4 sample displayed a completely agglomerated spherical morphology, with a determined average diameter of 15.37 nm .

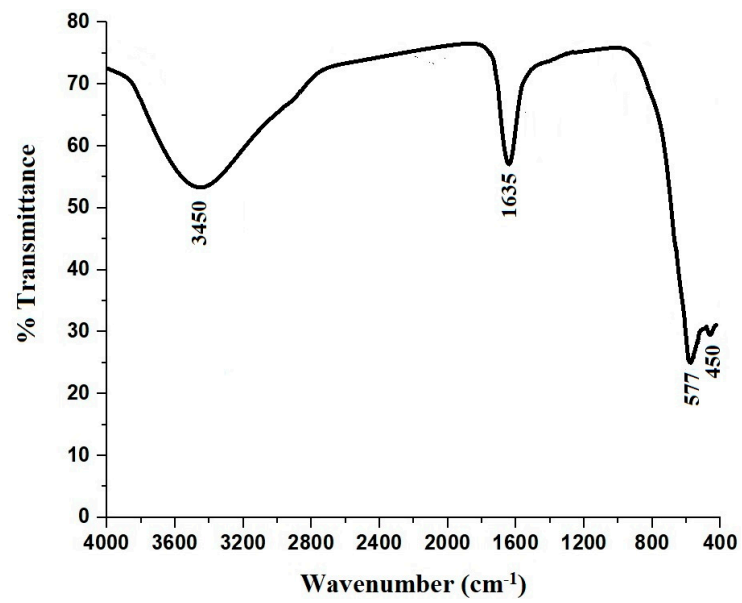


Figure 3. FTIR analysis of CoFe₂O₄ nanoparticles.

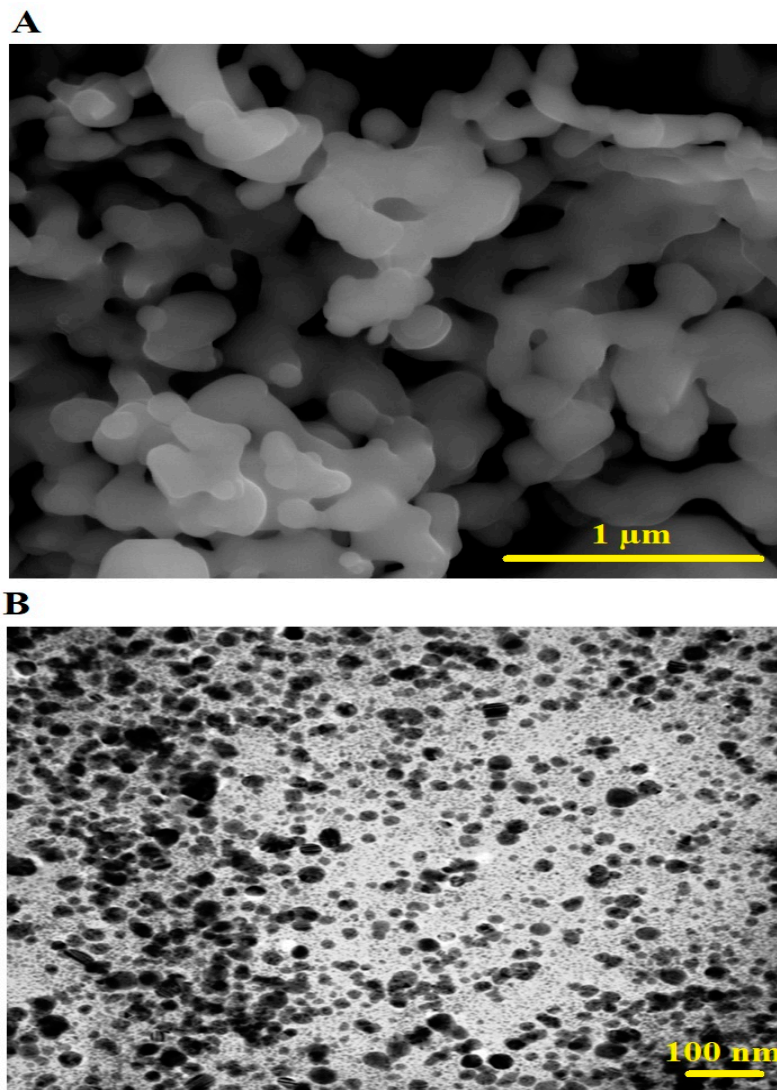


Figure 4. Characterization of CoFe₂O₄ nanoparticles using SEM (A) and TEM (B) analyses.

The EDS spectrum, depicted in Figure 5, demonstrates that the CoFe_2O_4 nanoparticles consisted of the elements Co, O, and Fe, with weight percentages of 17.82%, 32.72%, and 49.46%, respectively.

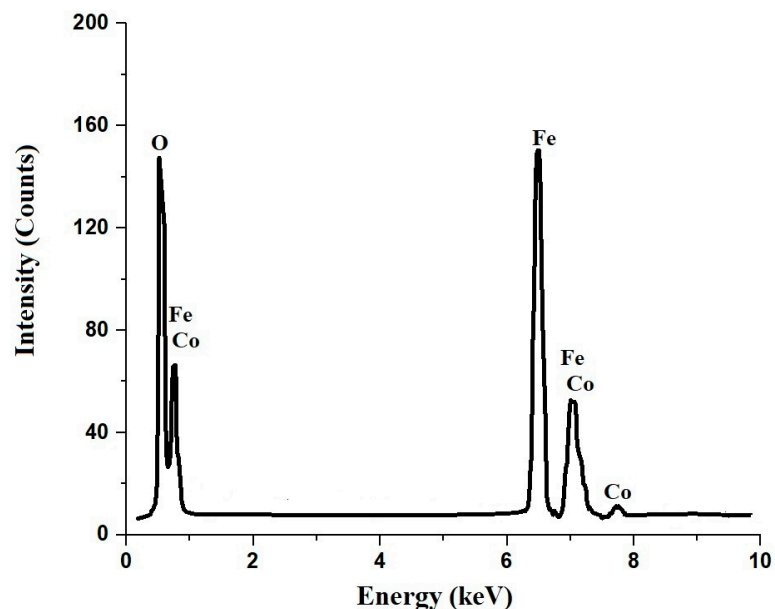


Figure 5. Characterization of CoFe_2O_4 nanoparticles using EDS analysis.

Figure 6 illustrates the N_2 adsorption/desorption isotherm of the CoFe_2O_4 nanoparticles. The results show that the resulting curve follows the IV type, and this confirms their mesoporous nature. Their surface textures, that is, their BET surface area, total pore volume, and average pore size, were found to be $59.65 \text{ m}^2/\text{g}$, 0.1234 cc/g , and 4.15 nm , respectively.

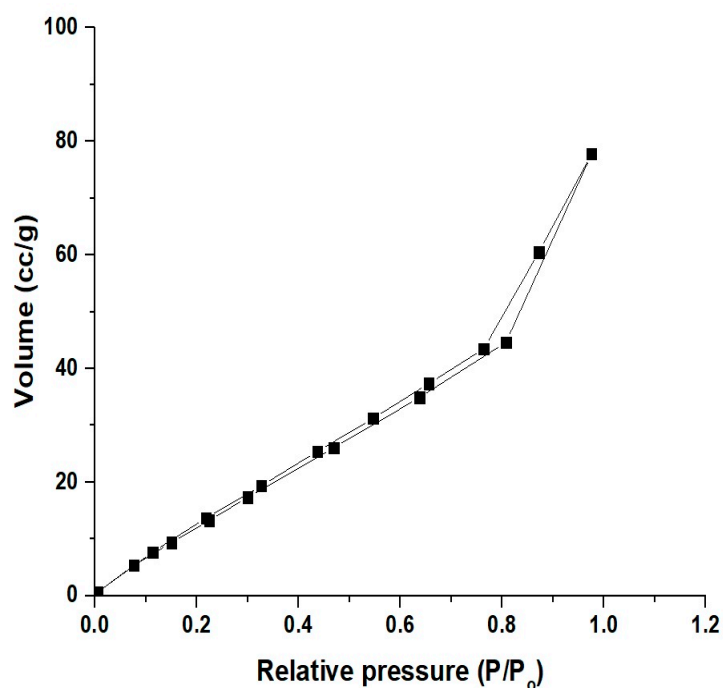


Figure 6. Characterization of CoFe_2O_4 nanoparticles using N_2 adsorption/desorption analysis.

3.2. Adsorption of Indigo Carmine Dye from Aqueous Solutions

3.2.1. Influence of pH

Figure 7A depicts the correlation between the elimination percentage of indigo carmine dye and the pH level of the solution. It was evident that a solution with a pH of 2 favored the removal process, yielding the highest removal efficiency at 82.98%. With an increase in solution pH, a consistent reduction in removal efficiency was observed, reaching 2.80% at a pH of 10. Consequently, a solution pH of 2 was selected as the optimal condition for subsequent adsorption investigations. In Figure 7B, the point of zero charge (pH_{PZC}) for the $CoFe_2O_4$ nanoparticles was determined to be 4.92. If the solution pH surpassed the point of zero charge (i.e., 4.92), the $CoFe_2O_4$ nanoparticle surface acquired a negative charge due to the presence of OH^- ions, resulting in a repulsion force between the anionic indigo carmine dye and the negatively charged adsorbent surface, as shown in Scheme 2. This led to a significant decrease in removal efficiency [5,6,26]. Conversely, when the solution pH was below the point of zero charge (i.e., 4.92), the surface of the $CoFe_2O_4$ nanoparticles became positively charged due to the presence of H^+ ions, causing an attraction force between the anionic indigo carmine dye and the positively charged adsorbent surface, as shown in Scheme 2. Consequently, a notable increase in removal efficiency was observed [5,6,26].

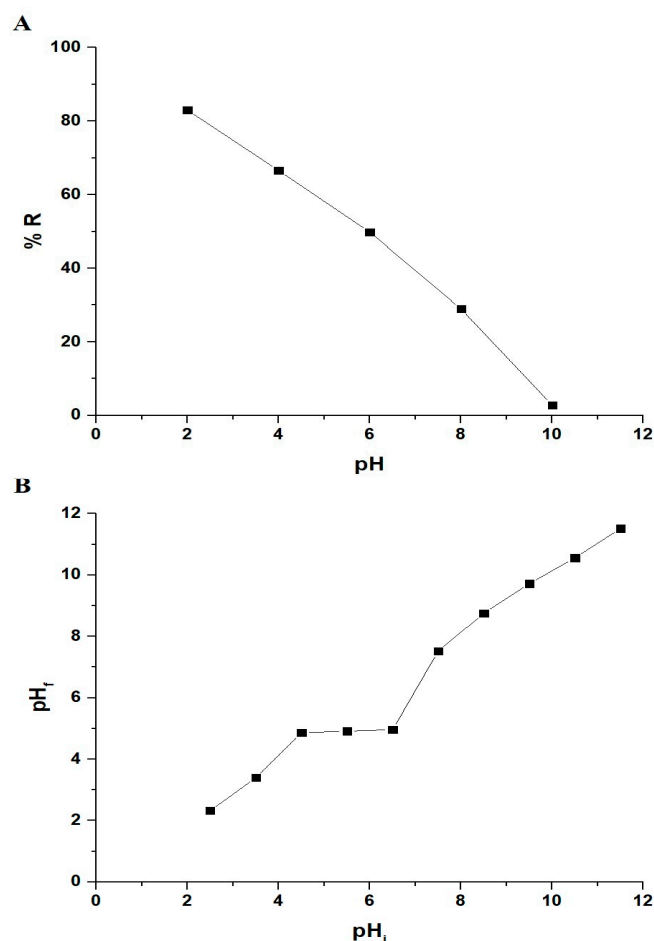
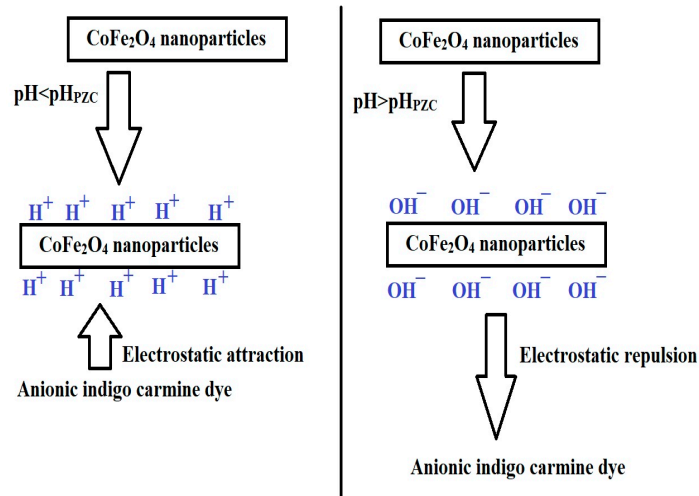


Figure 7. Variation of indigo carmine dye removal efficiency (% R) as a function of solution pH (A). The point of zero charge of $CoFe_2O_4$ nanoparticles (B).

Figure 4A illustrates the spherical shapes of the $CoFe_2O_4$ nanoparticles prior to adsorption. Following the adsorption of indigo carmine dye, as depicted in Figure 8, noticeable alterations in the surface morphology of the $CoFe_2O_4$ nanoparticles were observed in the SEM image. The adsorbate, representing the substance that underwent adsorption, adhered to the surface of the adsorbent, manifesting as a coating or deposit.



Scheme 2. Removal mechanism of indigo carmine dye by CoFe_2O_4 nanoparticles.

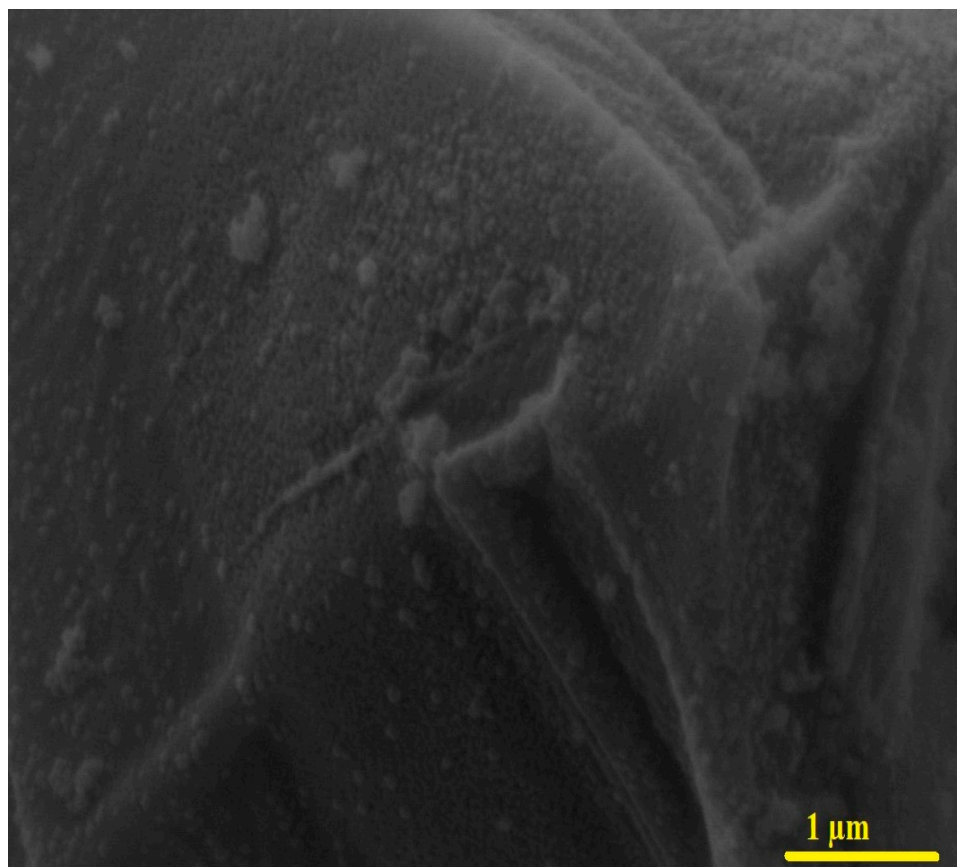


Figure 8. SEM image of the CoFe_2O_4 nanoparticles after the adsorption of indigo carmine dye.

3.2.2. Influence of Adsorption Time and Adsorption Kinetics

Figure 9A illustrates the changes in indigo carmine dye removal percentage over time. The findings unequivocally indicate a rapid removal rate, with indigo carmine dye removal efficiency rising from 51.5% to 82.65% as the removal time extended from 10 to 90 min, primarily attributed to the presence of protonated CoFe_2O_4 nanoparticles. Subsequently, as the removal time extended from 90 to 140 min, the adsorption percentage experienced a slight decline, as a consequence of reaching equilibrium because of the saturation of active places on the CoFe_2O_4 nanoparticles.

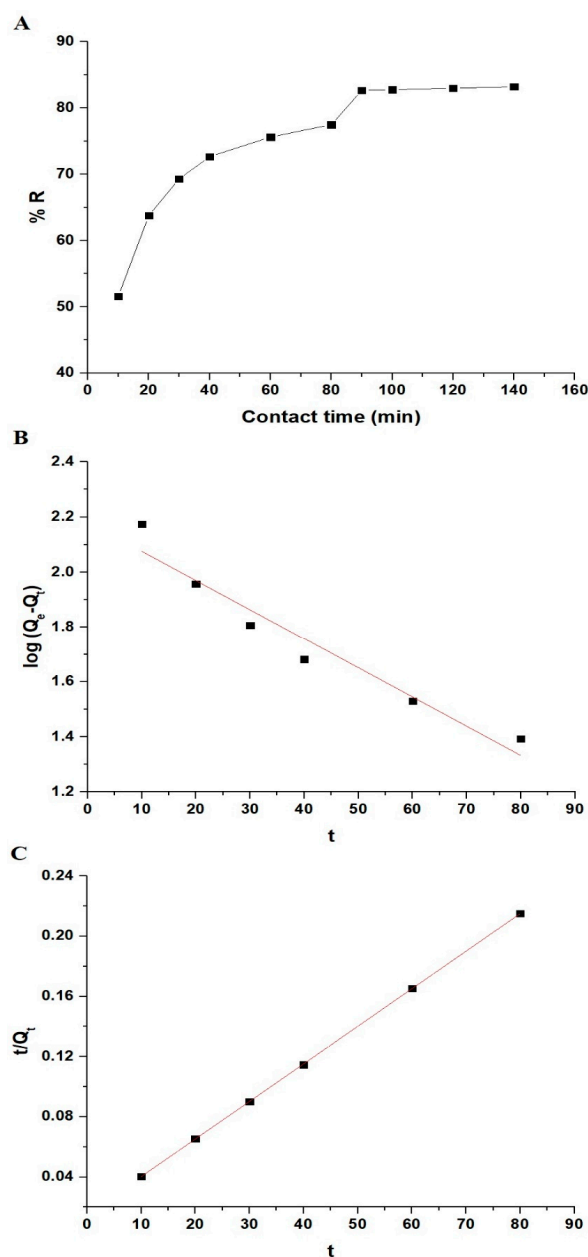


Figure 9. Variation of indigo carmine dye removal efficiency (% R) as a function of contact time (A). The pseudo-first-order (B) and pseudo-second-order (C) kinetic models.

In this study, we applied both the pseudo-first-order and pseudo-second-order models to investigate the kinetics. Equations (3) and (4) present the linear forms of these models, respectively [5,6,26].

$$\log(Q_e - Q_t) = \log Q_e - \frac{k_{First} t}{2.303} \quad (3)$$

$$\frac{t}{Q_t} = \frac{1}{k_{Second} Q_e^2} + \frac{1}{Q_e} t \quad (4)$$

Q_t represents the quantity of indigo carmine dye eliminated by the CoFe_2O_4 nanoparticles at a specific contact time, denoted as t (mg/g). On the other hand, Q_e stands for the amount of indigo carmine dye removed by the CoFe_2O_4 adsorbent at equilibrium (mg/g). The value k_{First} is used to denote the rate constant of the pseudo-first-order model (1/min), while k_{Second} represents the rate constant of the pseudo-second-order model (g/mg min).

Figure 9B presents the alignment of experimental data with the pseudo-first-order kinetic model, while Figure 9C illustrates the alignment with the pseudo-second-order kinetic model. Table 2 represents a summary of critical kinetic parameters obtained by fitting experimental data with these two distinct kinetic models. The table highlights that the R^2 value for the pseudo-second-order kinetic model exceeds that of the pseudo-first-order kinetic model. Furthermore, a clear agreement between the experimental adsorption capacity (Q_{exp}) and the model-predicted values emphasizes the concordance between the experimental and pseudo-second-order model adsorption capacities. These observations confirm the applicability of the pseudo-second-order kinetic model to this removal process, providing strong evidence for the occurrence of chemisorption between indigo carmine dye molecules and $CoFe_2O_4$ nanoparticles.

Table 2. Kinetic constants of indigo carmine dye removal by $CoFe_2O_4$ nanoparticles.

Experimental		Pseudo-First-Order		Pseudo-Second-Order		
Q_{exp} (mg/g)	Q_e (mg/g)	k_{First} (1/min)	R^2	Q_e (mg/g)	k_{Second} (g/mg·min)	R^2
396.74	152.06	0.0245	0.9300	400.00	0.00041	0.9999

3.2.3. Influence of Solution Temperature and Thermodynamic Parameters

Figure 10A depicts the changes in the indigo carmine dye removal percentage concerning temperature. The findings indicate a noticeable decline in indigo carmine dye uptake efficiency, decreasing from 82.65% to 45.73% as the adsorption temperature rose from 298 to 328 K. In order to explore the role of adsorption temperature on the process of removing indigo carmine dye by $CoFe_2O_4$ nanoparticles, the standard entropy change (ΔS°), standard enthalpy change (ΔH°), and standard Gibbs free energy change (ΔG°) were calculated using Equations (5)–(7) [5,6,26].

$$\ln K_d = \frac{\Delta S^\circ}{R} - \frac{\Delta H^\circ}{RT} \quad (5)$$

$$\Delta G^\circ = \Delta H^\circ - T\Delta S^\circ \quad (6)$$

$$K_d = \frac{Q_e}{C_{eq}} \quad (7)$$

T stands for the adsorption temperature (K), with R denoting the universal gas constant (KJ/molK), and K_d representing the distribution coefficient (given in L/g). The values of ΔS° and ΔH° were determined by analyzing the intercept and slope of the plot of $\ln K_d$ against $1/T$, as illustrated in Figure 10B. The resulting thermodynamic constants are detailed in Table 3. Negative ΔG° values confirm the spontaneity of the indigo carmine dye removal process by $CoFe_2O_4$ nanoparticles. The obtained ΔH° value of -47.82 KJ/mol confirms that the removal process was exothermic, and with a value exceeding 40 KJ/mol, this indicates that the removal process predominantly involved chemisorption. Additionally, the positive ΔS° value (0.1415 KJ/molK) is associated with an increase in the degree of freedom of indigo carmine dye and suggests an enhanced concentration of indigo carmine dye at the solid–solution interface [5,6,26].

Table 3. Thermodynamic constants of indigo carmine dye removal by $CoFe_2O_4$ nanoparticles.

ΔH° (KJ/mol)	ΔS° (KJ/mol K)	ΔG° (KJ/mol)			
−47.82	0.1415	298	308	318	328
		−89.99	−91.41	−92.83	−94.24

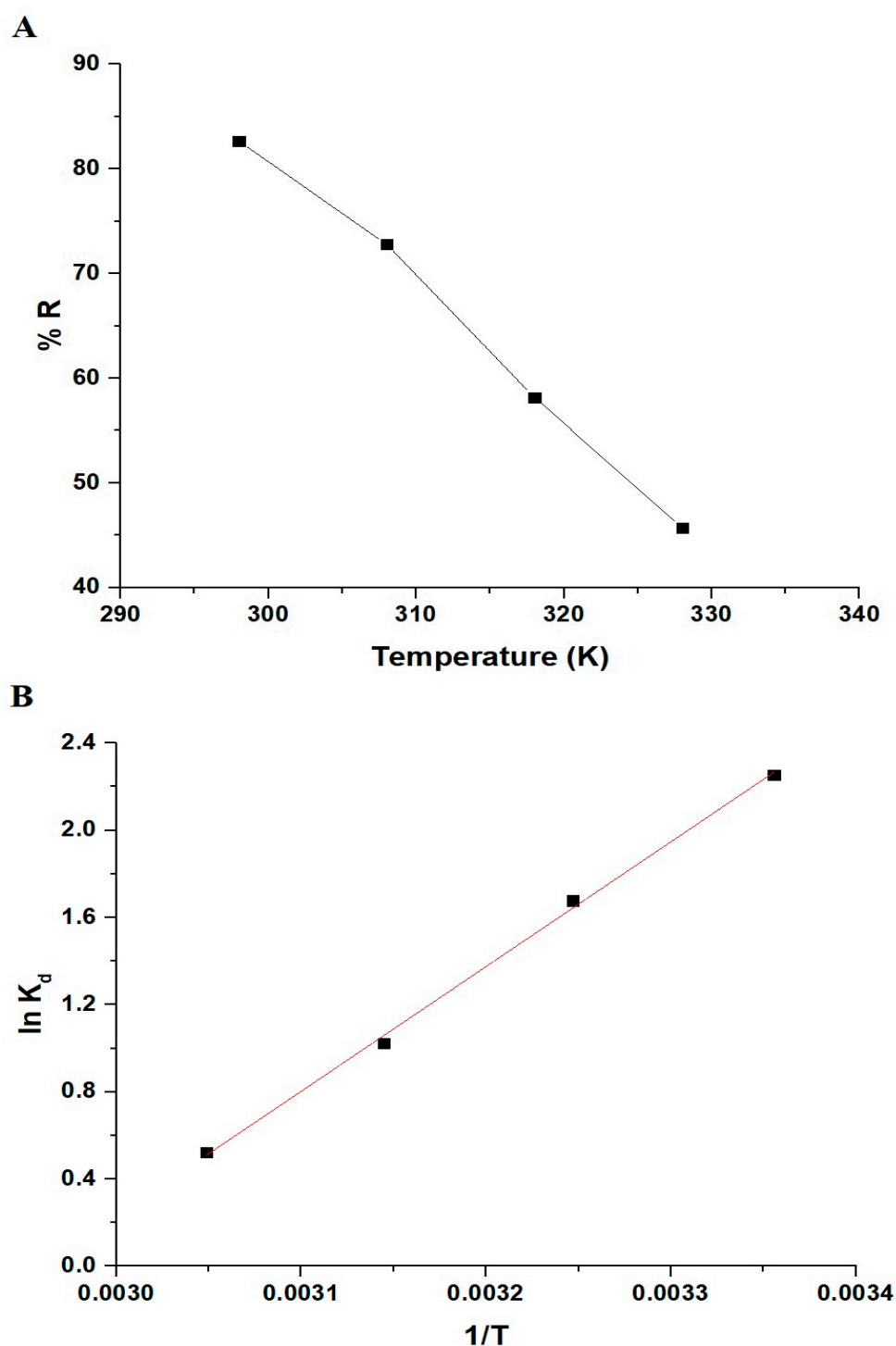


Figure 10. Variation of indigo carmine dye removal efficiency (% R) as a function of temperature (A). The plot of $\ln K_d$ versus $1/T$ (B).

3.2.4. Influence of Concentration and Adsorption Isotherms

Figure 11A presents the changes in the indigo carmine dye removal percentage in relation to the initial dye concentration. The results unequivocally illustrate a decrease in the indigo carmine dye removal percentage, declining from 98.38% to 71.34% as the initial indigo carmine dye concentration increased from 40 to 280 mg/L. This can be attributed to the presence of unsaturated active sites on the adsorbent at lower dye concentrations of adsorbate, while at higher dye concentrations of adsorbate, it is conceivable that all active sites of the adsorbent became saturated.

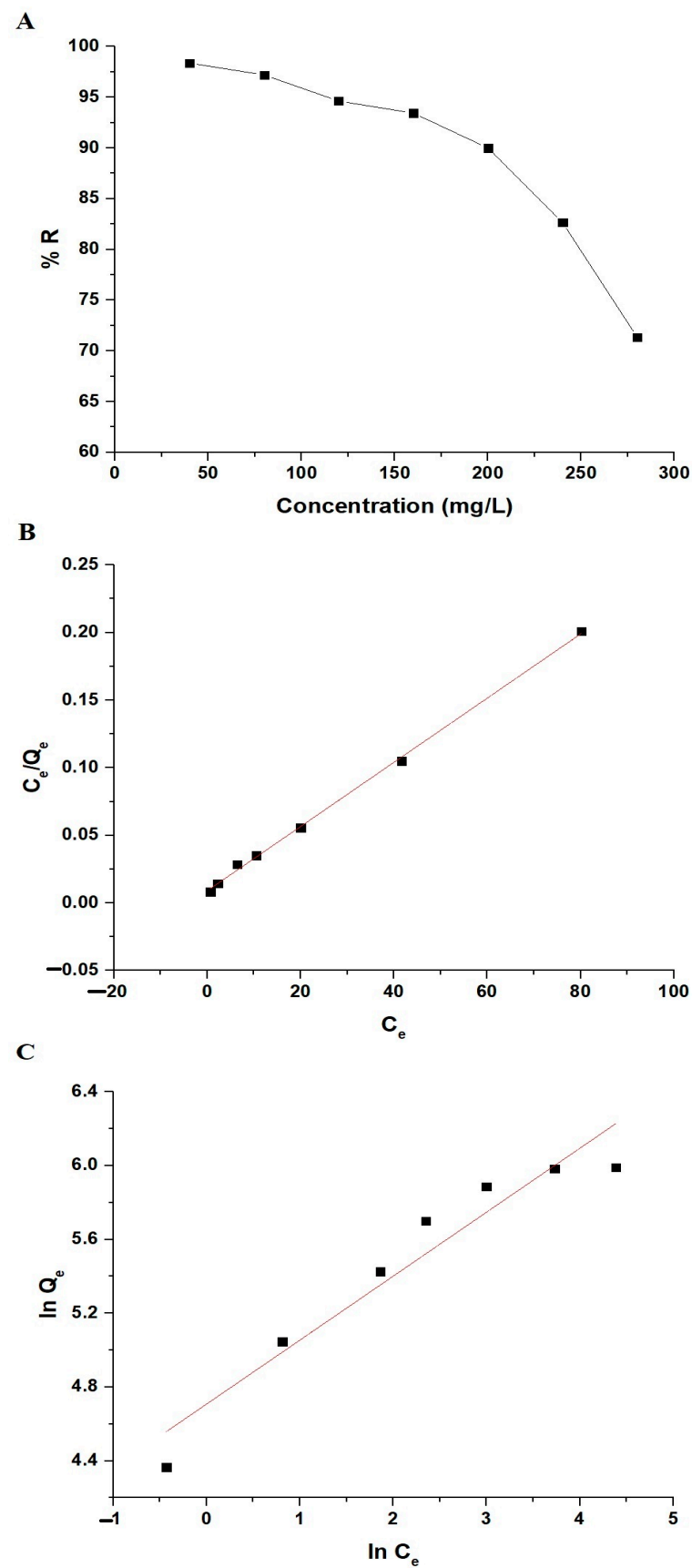


Figure 11. Variation of indigo carmine dye removal efficiency (% R) as a function of initial dye concentration (A). The Langmuir (B) and Freundlich (C) equilibrium isotherms.

In this study, the equilibrium analysis was carried out using the Langmuir and Freundlich isotherms. Equations (8) and (9) present the linear representations of these equilibrium isotherms, respectively [5,6,26].

$$\frac{C_{eq}}{Q_e} = \frac{1}{k_L Q_{max}} + \frac{C_{eq}}{Q_{max}} \quad (8)$$

$$\ln Q_e = \ln k_F + \frac{1}{n} \ln C_{eq} \quad (9)$$

The parameter $1/n$ represents the degree of heterogeneity, while k_L denotes the Langmuir constant (L/mg). Additionally, k_F is used to represent the Freundlich constant $(\text{mg/g})(\text{L/mg})^{1/n}$, and Q_{max} signifies the maximum adsorption capacity as per the Langmuir isotherm (mg/g). It is worth noting that Q_{max} can also be calculated using Equation (10) based on the Freundlich isotherm [5,6,26].

$$Q_{max} = k_F \left(C_0^{1/n} \right) \quad (10)$$

Figure 11B demonstrates the alignment of experimental data with the Langmuir equilibrium isotherm, and Figure 11C showcases the alignment with the Freundlich equilibrium isotherm. In Table 4, there is a summary of key equilibrium constants derived from the linear fitting of experimental data using these two distinct equilibrium isotherms. The table highlights that the R^2 value for the Langmuir equilibrium isotherm exceeds that of the Freundlich equilibrium isotherm. As a result, these findings support the applicability of the Langmuir equilibrium isotherm to this adsorption process.

Table 4. Equilibrium constants of indigo carmine dye removal by CoFe_2O_4 nanoparticles.

Langmuir Isotherm			Freundlich Isotherm		
Q_{max} (mg/g)	k_L (L/mg)	R^2	Q_{max} (mg/g)	k_F (mg/g)(L/mg) ^{1/n}	R^2
421.94	0.2596	0.9985	740.01	110.85	0.9148

The analysis of the Langmuir isotherm revealed a maximum adsorption capacity of 421.94 mg/g for indigo carmine dye on CoFe_2O_4 nanoparticles. When assessing this maximum adsorption capacity, a comparison was made between the adsorption performance of indigo carmine dye on CoFe_2O_4 nanoparticles and that of various adsorbents listed in Table 5. The results unequivocally indicate that the synthesized CoFe_2O_4 nanoparticles exhibited a superior adsorption capacity for indigo carmine dye in comparison to previously reported adsorbents, including polyacrylonitrile/ Fe_3O_4 /3-mercaptopropionic acid composite, activated carbon, montmorillonite, chitosan aerogels, and carbon nanotubes [35,37–40].

Table 5. A comparison between the maximum removal capacity of CoFe_2O_4 nanoparticles towards indigo carmine dye and that of other previously documented adsorbents.

Adsorbent	Maximum Adsorption Capacity (mg/g)	pH	Time	Ref.
Polyacrylonitrile/ Fe_3O_4 /3-mercaptopropionic acid composite	154.50	5	25	[37]
Activated carbon	87.80	2	80	[35]
Montmorillonite	40.00	2	20	[38]
Chitosan aerogels	168.60	2	100	[39]
Carbon nanotubes	93.00	2	50	[40]
CoFe_2O_4 nanoparticles	421.94	2	90	This study

3.2.5. Influence of Regeneration and Reusability

The regeneration of adsorbents is crucial for their continued effectiveness in various processes. Adsorbents are materials that trap and remove impurities from gases or liquids. Over time, these adsorbents can become saturated with contaminants, reducing their efficiency. Regeneration helps restore their adsorption capacity and extends their lifespan. This is particularly important in industries such as water treatment, air purification, and gas separation, where maintaining high performance is essential for cost-effectiveness and environmental sustainability. It also allows for the reuse of adsorbents, reducing the need for frequent replacement and minimizing waste generation. So, in a nutshell, regeneration is like giving a second life to these materials, ensuring they can continue to effectively clean and purify substances. To regenerate the CoFe_2O_4 nanoparticles for multiple uses, the CoFe_2O_4 /indigo carmine dye mixture was subjected to heating at $600\text{ }^\circ\text{C}$, which broke down and removed the dye. Subsequently, the regenerated CoFe_2O_4 adsorbent was utilized for the successive removal of indigo carmine dye in five consecutive cycles, following the same experimental procedure described earlier and depicted in Figure 12. The outcomes illustrated the capability of CoFe_2O_4 nanoparticles to repeatedly eliminate indigo carmine dye without experiencing a significant reduction in efficiency.

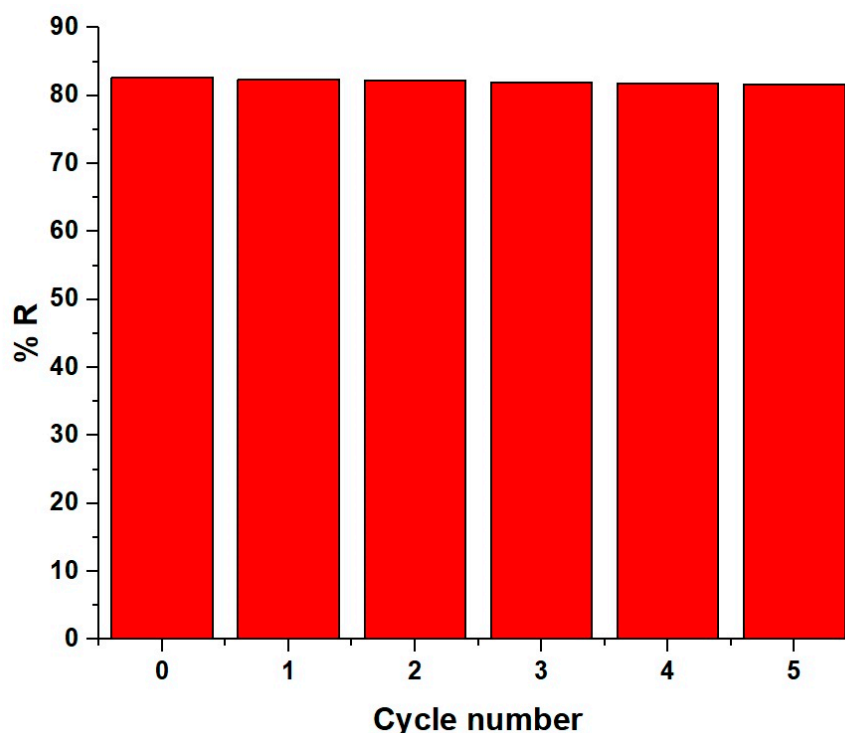


Figure 12. Influence of reusability of CoFe_2O_4 nanoparticles for the elimination of indigo carmine dye.

4. Conclusions

This research involved the straightforward synthesis of CoFe_2O_4 nanoparticles using the Pechini sol-gel technique. These nanoparticles were then employed as an adsorbent to efficiently eliminate indigo carmine dye from aqueous solutions. The maximum adsorption capacity of CoFe_2O_4 for indigo carmine dye was determined to be 421.94 mg/g . XRD analysis revealed that the average crystallite size of the CoFe_2O_4 nanoparticles was 18.75 nm . A closer examination through scanning electron microscopy (SEM) showed that these nanoparticles exhibited a nearly spherical, ball-like morphology with an average grain size of 198.32 nm . Besides that, transmission electron microscopy (TEM) analysis demonstrated that the CoFe_2O_4 nanoparticles displayed a fully agglomerated spherical structure with an average diameter of 15.37 nm . The removal of indigo carmine dye by CoFe_2O_4 is characterized as spontaneous, exothermic, and chemical. Also, it is well described by the

Langmuir equilibrium isotherm and the pseudo-second-order kinetic model. The optimal conditions for the removal of indigo carmine dye by CoFe_2O_4 nanoparticles were observed at a pH of 2, a contact time of 90 min, and an adsorption temperature of 298 K.

Author Contributions: A.S.A.-W. (review, writing of the introduction, and interpretation of the kinetic and equilibrium parts) and E.A.A. (writing, review, idea, experimental work, and analysis). All authors have read and agreed to the published version of the manuscript.

Funding: This research was funded by Princess Nourah bint Abdulrahman University Researchers Supporting Project number (PNURSP2023R35), Princess Nourah bint Abdulrahman University, Riyadh, Saudi Arabia.

Institutional Review Board Statement: The authors ensure that the paper hereby submitted is completely original and has not been previously published in any format or language, either partially or in its complete form anywhere else. This study was conducted and approved according to the guidelines of the Declaration of the Ethical Committee of the Faculty of Science, Benha University (No. BuFs-REC-2023-76 Chm).

Data Availability Statement: Every dataset produced or scrutinized within the scope of this research is incorporated in this article.

Acknowledgments: The authors are grateful to Princess Nourah bint Abdulrahman University, Riyadh, Saudi Arabia for funding this work through Researchers Supporting Project number (PNURSP2023R35).

Conflicts of Interest: All the authors declare that there are no potential conflict of interest associated with this paper.

References

1. El-Kordy, A.; Elgamouz, A.; Lemdek, E.M.; Tijani, N.; Alharthi, S.S.; Kawde, A.N.; Shehadi, I. Preparation of Sodalite and Faujasite Clay Composite Membranes and Their Utilization in the Decontamination of Dye Effluents. *Membranes* **2022**, *12*, 12. [[CrossRef](#)] [[PubMed](#)]
2. Akrami, M.; Danesh, S.; Eftekhari, M. Comparative Study on the Removal of Cationic Dyes Using Different Graphene Oxide Forms. *J. Inorg. Organomet. Polym. Mater.* **2019**, *29*, 1785–1797. [[CrossRef](#)]
3. Ghiasi, E.; Malekzadeh, A. Removal of Various Textile Dyes Using $\text{LaMn}(\text{Fe})\text{O}_3$ and $\text{LaFeMn}_{0.5}\text{O}_3$ Nanoperovskites; RSM Optimization, Isotherms and Kinetics Studies. *J. Inorg. Organomet. Polym. Mater.* **2020**, *30*, 2789–2804. [[CrossRef](#)]
4. Ma, T.; Wu, Y.; Liu, N.; Wu, Y. Iron Manganese Oxide Modified Multi-Walled Carbon Nanotube as Efficient Adsorbent for Removal of Organic Dyes: Performance, Kinetics and Mechanism Studies. *J. Inorg. Organomet. Polym. Mater.* **2020**, *30*, 4027–4042. [[CrossRef](#)]
5. Abdelrahman, E.A.; Algethami, F.K.; Alsalem, H.S.; Binkadem, M.S. Facile Synthesis and Characterization of Novel Nanostructures for the Efficient Disposal of Crystal Violet Dye from Aqueous Media. *Inorganics* **2023**, *11*, 339. [[CrossRef](#)]
6. Abdelrahman, E.A.; Algethami, F.K.; AlSalem, H.S.; Binkadem, M.S.; Khairy, M.; Saad, F.A.; El-Sayyad, G.S.; Alqahtani, Z. Efficient Disposal of Rhodamine 6G and Acid Orange 10 Dyes from Aqueous Media Using $\text{ZrO}_2/\text{CdMn}_2\text{O}_4/\text{CdO}$ as Novel and Facilely Synthesized Nanocomposites. *Inorganics* **2023**, *11*, 333. [[CrossRef](#)]
7. Liu, Y.; Zhao, Y.; Cheng, W.; Zhang, T. Targeted Reclaiming Cationic Dyes from Dyeing Wastewater with a Dithiocarbamate-Functionalized Material through Selective Adsorption and Efficient Desorption. *J. Colloid Interface Sci.* **2020**, *579*, 766–777. [[CrossRef](#)]
8. Sirajudheen, P.; Karthikeyan, P.; Vigneshwaran, S.; Nikitha, M.; Hassan, C.A.A.; Meenakshi, S. Ce(III) Networked Chitosan/ β -Cyclodextrin Beads for the Selective Removal of Toxic Dye Molecules: Adsorption Performance and Mechanism. *Carbohydr. Polym. Technol. Appl.* **2020**, *1*, 100018. [[CrossRef](#)]
9. Rafiq, A.; Imran, M.; Aqeel, M.; Naz, M.; Ikram, M.; Ali, S. Study of Transition Metal Ion Doped CdS Nanoparticles for Removal of Dye from Textile Wastewater. *J. Inorg. Organomet. Polym. Mater.* **2020**, *30*, 1915–1923. [[CrossRef](#)]
10. Ahmed, N.A.; Elshahawy, M.F.; Mohammed, R.D.; Mahmoud, G.A. Removal of Astrazon Red Dye from Wastewater Using Eggshell/Graphene Oxide Embed in (Gum Acacia/Acrylamide) Hydrogel Nanocomposites Synthesized by Gamma Irradiation. *J. Inorg. Organomet. Polym. Mater.* **2023**, *33*, 3617–3637. [[CrossRef](#)]
11. Fathi, E.; Derakhshanfard, F.; Gharbani, P.; Ghazi Tabatabaei, Z. Facile Synthesis of $\text{MgO}/\text{C}_3\text{N}_4$ Nanocomposite for Removal of Reactive Orange 16 Under Visible Light. *J. Inorg. Organomet. Polym. Mater.* **2020**, *30*, 2234–2240. [[CrossRef](#)]
12. Noreen, S.; Khalid, U.; Ibrahim, S.M.; Javed, T.; Ghani, A.; Naz, S.; Iqbal, M. ZnO, MgO and FeO Adsorption Efficiencies for Direct Sky Blue Dye: Equilibrium, Kinetics and Thermodynamics Studies. *J. Mater. Res. Technol.* **2020**, *9*, 5881–5893. [[CrossRef](#)]
13. Kumar, N.; Pandey, A.; Rosy; Sharma, Y.C. A Review on Sustainable Mesoporous Activated Carbon as Adsorbent for Efficient Removal of Hazardous Dyes from Industrial Wastewater. *J. Water Process Eng.* **2023**, *54*, 104054. [[CrossRef](#)]

14. Ahmadian, M.; Jaymand, M. Interpenetrating Polymer Network Hydrogels for Removal of Synthetic Dyes: A Comprehensive Review. *Coord. Chem. Rev.* **2023**, *486*, 215152. [[CrossRef](#)]
15. Kausar, A.; Zohra, S.T.; Ijaz, S.; Iqbal, M.; Iqbal, J.; Bibi, I.; Nouren, S.; El Messaoudi, N.; Nazir, A. Cellulose-Based Materials and Their Adsorptive Removal Efficiency for Dyes: A Review. *Int. J. Biol. Macromol.* **2023**, *224*, 1337–1355. [[CrossRef](#)]
16. Singh, B.; Singh, P.; Siddiqui, S.; Singh, D.; Gupta, M. Wastewater Treatment Using Fe-Doped Perovskite Manganites by Photocatalytic Degradation of Methyl Orange, Crystal Violet and Indigo Carmine Dyes in Tungsten Bulb/Sunlight. *J. Rare Earths* **2023**, *41*, 1311–1322. [[CrossRef](#)]
17. Bakry, A.M.; Alamier, W.M.; El-Shall, M.S.; Awad, F.S. Facile Synthesis of Amorphous Zirconium Phosphate Graphitic Carbon Nitride Composite and Its High Performance for Photocatalytic Degradation of Indigo Carmine Dye in Water. *J. Mater. Res. Technol.* **2022**, *20*, 1456–1469. [[CrossRef](#)]
18. Roy, H.; Rahman, T.U.; Khan, M.A.J.R.; Al-Mamun, M.R.; Islam, S.Z.; Khaleque, M.A.; Hossain, M.I.; Khan, M.Z.H.; Islam, M.S.; Marwani, H.M.; et al. Toxic Dye Removal, Remediation, and Mechanism with Doped SnO₂-Based Nanocomposite Photocatalysts: A Critical Review. *J. Water Process Eng.* **2023**, *54*, 104069. [[CrossRef](#)]
19. Venkatesh, D.; Pavalamalar, S.; Anbalagan, K. Selective Photodegradation on Dual Dye System by Recoverable Nano SnO₂ Photocatalyst. *J. Inorg. Organomet. Polym. Mater.* **2019**, *29*, 939–953. [[CrossRef](#)]
20. Zhao, J.; Dang, Z.; Muddassir, M.; Raza, S.; Zhong, A.; Wang, X.; Jin, J. A New Cd(II)-Based Coordination Polymer for Efficient Photocatalytic Removal of Organic Dyes. *Molecules* **2023**, *28*, 6848. [[CrossRef](#)]
21. Zheng, M.; Chen, J.; Zhang, L.; Cheng, Y.; Lu, C.; Liu, Y.; Singh, A.; Trivedi, M.; Kumar, A.; Liu, J. Metal Organic Frameworks as Efficient Adsorbents for Drugs from Wastewater. *Mater. Today Commun.* **2022**, *31*, 103514. [[CrossRef](#)]
22. Liu, Y.; Tan, Y.; Cheng, Z.; Liu, S.; Ren, Y.; Chen, X.; Fan, M.; Shen, Z. Quantitative Structure-Activity Relationship (QSAR) Guides the Development of Dye Removal by Coagulation. *J. Hazard. Mater.* **2022**, *438*, 129448. [[CrossRef](#)] [[PubMed](#)]
23. Hou, K.; Jin, K.; Fan, Z.; Du, P.; Ji, Y.; Wang, J.; Zhao, Y.; Yao, C.; Cai, Z. Facile Fabrication of Fabric-Based Membrane for Adjustable Oil-in-Water Emulsion Separation, Suspension Filtration and Dye Removal. *Sep. Purif. Technol.* **2023**, *323*, 124467. [[CrossRef](#)]
24. Wu, S.; Shi, W.; Li, K.; Cai, J.; Xu, C.; Gao, L.; Lu, J.; Ding, F. Chitosan-Based Hollow Nanofiber Membranes with Polyvinylpyrrolidone and Polyvinyl Alcohol for Efficient Removal and Filtration of Organic Dyes and Heavy Metals. *Int. J. Biol. Macromol.* **2023**, *239*, 124264. [[CrossRef](#)]
25. Gurav, R.; Bhatia, S.K.; Choi, T.R.; Choi, Y.K.; Kim, H.J.; Song, H.S.; Lee, S.M.; Lee Park, S.; Lee, H.S.; Koh, J.; et al. Application of Macroalgal Biomass Derived Biochar and Bioelectrochemical System with Shewanella for the Adsorptive Removal and Biodegradation of Toxic Azo Dye. *Chemosphere* **2021**, *264*, 128539. [[CrossRef](#)]
26. Al-Wasidi, A.S.; Khairy, M.; Abdulkhair, B.Y.; Abdelrahman, E.A. Efficient Disposal of Basic Fuchsin Dye from Aqueous Media Using ZrO₂/MgMn₂O₄/Mg(Mg_{0.333}Mn_{1.333})O₄ as a Novel and Facilely Synthesized Nanocomposite. *Inorganics* **2023**, *11*, 363. [[CrossRef](#)]
27. Li, L.; Zou, J.; Han, Y.; Liao, Z.; Lu, P.; Nezamzadeh-Ejehieh, A.; Liu, J.; Peng, Y. Recent Advances in Al(III)/In(III)-Based MOFs for the Detection of Pollutants. *New J. Chem.* **2022**, *46*, 19577–19592. [[CrossRef](#)]
28. Li, Z.; Sellaoui, L.; Franco, D.; Netto, M.S.; Georgin, J.; Dotto, G.L.; Bajahzar, A.; Belmabrouk, H.; Bonilla-Petriciolet, A.; Li, Q. Adsorption of Hazardous Dyes on Functionalized Multiwalled Carbon Nanotubes in Single and Binary Systems: Experimental Study and Physicochemical Interpretation of the Adsorption Mechanism. *Chem. Eng. J.* **2020**, *389*, 124467. [[CrossRef](#)]
29. Feng, C.; Ren, P.; Huo, M.; Dai, Z.; Liang, D.; Jin, Y.; Ren, F. Facile Synthesis of Trimethylammonium Grafted Cellulose Foams with High Capacity for Selective Adsorption of Anionic Dyes from Water. *Carbohydr. Polym.* **2020**, *241*, 116369. [[CrossRef](#)]
30. Tambat, S.N.; Ahirrao, D.J.; Pandit, A.B.; Jha, N.; Sontakke, S.M. Hydrothermally Synthesized N₂-UiO-66 for Enhanced and Selective Adsorption of Cationic Dyes. *Environ. Technol. Innov.* **2020**, *19*, 101021. [[CrossRef](#)]
31. Sirajudheen, P.; Karthikeyan, P.; Vigneshwaran, S.; Meenakshi, S. Synthesis and Characterization of La(III) Supported Carboxymethylcellulose-Clay Composite for Toxic Dyes Removal: Evaluation of Adsorption Kinetics, Isotherms and Thermodynamics. *Int. J. Biol. Macromol.* **2020**, *161*, 1117–1126. [[CrossRef](#)]
32. Yao, X.; Ji, L.; Guo, J.; Ge, S.; Lu, W.; Chen, Y.; Cai, L.; Wang, Y.; Song, W. An Abundant Porous Biochar Material Derived from Wakame (*Undaria pinnatifida*) with High Adsorption Performance for Three Organic Dyes. *Bioresour. Technol.* **2020**, *318*, 124082. [[CrossRef](#)]
33. Zhang, J.; Zhou, Q.; Ou, L. Removal of Indigo Carmine from Aqueous Solution by Microwave-Treated Activated Carbon from Peanut Shell. *Desalin. Water Treat.* **2016**, *57*, 718–727. [[CrossRef](#)]
34. Nakamura, T.; Kawasaki, N.; Tanada, S.; Tamura, T.; Shimizu, Y. Indigo Carmine Removal by Charcoal from Rice Bran as an Agricultural By-Product. *Toxicol. Environ. Chem.* **2005**, *87*, 321–327. [[CrossRef](#)]
35. Kesraoui, A.; Selmi, T.; Seffen, M.; Brouers, F. Influence of Alternating Current on the Adsorption of Indigo Carmine. *Environ. Sci. Pollut. Res.* **2017**, *24*, 9940–9950. [[CrossRef](#)] [[PubMed](#)]
36. Jiwalak, N.; Rattanaphani, S.; Bremner, J.B.; Rattanaphani, V. Equilibrium and Kinetic Modeling of the Adsorption of Indigo Carmine onto Silk. *Fibers Polym.* **2010**, *11*, 572–579. [[CrossRef](#)]
37. Yazdi, M.G.; Ivanic, M.; Mohamed, A.; Uheida, A. Surface Modified Composite Nanofibers for the Removal of Indigo Carmine Dye from Polluted Water. *RSC Adv.* **2018**, *8*, 24588–24598. [[CrossRef](#)]

38. Geyikçi, F. Factorial Design Analysis for Adsorption of Indigo Carmine onto Montmorillonite-Evaluation of the Kinetics and Equilibrium Data. *Prog. Org. Coat.* **2016**, *98*, 28–34. [[CrossRef](#)]
39. De Luna, M.S.; Ascione, C.; Santillo, C.; Verdolotti, L.; Lavorgna, M.; Buonocore, G.G.; Castaldo, R.; Filippone, G.; Xia, H.; Ambrosio, L. Optimization of Dye Adsorption Capacity and Mechanical Strength of Chitosan Aerogels through Crosslinking Strategy and Graphene Oxide Addition. *Carbohydr. Polym.* **2019**, *211*, 195–203. [[CrossRef](#)]
40. Elamin, M.R.; Abdulkhair, B.Y.; Elzupir, A.O. Removal of Ciprofloxacin and Indigo Carmine from Water by Carbon Nanotubes Fabricated from a Low-Cost Precursor: Solution Parameters and Recyclability. *Ain Shams Eng. J.* **2022**, *14*, 101844. [[CrossRef](#)]
41. Kanwal, A.; Bhatti, H.N.; Iqbal, M.; Noreen, S. Basic Dye Adsorption onto Clay/MnFe₂O₄ Composite: A Mechanistic Study. *Water Environ. Res.* **2017**, *89*, 301–311. [[CrossRef](#)] [[PubMed](#)]
42. Adeogun, A.I. Removal of Methylene Blue Dye from Aqueous Solution Using Activated Charcoal Modified Manganese Ferrite (AC-MnFe₂O₄): Kinetics, Isotherms, and Thermodynamics Studies. *Part. Sci. Technol.* **2020**, *38*, 756–767. [[CrossRef](#)]
43. Al-Wasidi, A.S.; Algethami, F.K.; Saad, F.A.; Abdelrahman, E.A. Remarkable High Adsorption of Methylene Blue Dye from Aqueous Solutions Using Facilely Synthesized MgFe₂O₄ Nanoparticles. *J. Inorg. Organomet. Polym. Mater.* **2023**, *33*, 2035–2045. [[CrossRef](#)]
44. Adel, M.; Ahmed, M.A.; Mohamed, A.A. Synthesis and Characterization of Magnetically Separable and Recyclable Crumbled MgFe₂O₄/Reduced Graphene Oxide Nanoparticles for Removal of Methylene Blue Dye from Aqueous Solutions. *J. Phys. Chem. Solids* **2021**, *149*, 109760. [[CrossRef](#)]
45. Vergis, B.R.; Kottam, N.; Hari Krishna, R.; Nagabhushana, B.M. Removal of Evans Blue Dye from Aqueous Solution Using Magnetic Spinel ZnFe₂O₄ Nanomaterial: Adsorption Isotherms and Kinetics. *Nano-Struct. Nano-Objects* **2019**, *18*, 100290. [[CrossRef](#)]
46. Algarni, T.S.; Al-Mohaimeed, A.M.; Al-Odayni, A.B.; Abduh, N.A.Y. Activated Carbon/ZnFe₂O₄ Nanocomposite Adsorbent for Efficient Removal of Crystal Violet Cationic Dye from Aqueous Solutions. *Nanomaterials* **2022**, *12*, 3224. [[CrossRef](#)]
47. Li, Z.; Hanafy, H.; Zhang, L.; Sellaoui, L.; Schadeck Netto, M.; Oliveira, M.L.S.; Seliem, M.K.; Luiz Dotto, G.; Bonilla-Petriciolet, A.; Li, Q. Adsorption of Congo Red and Methylene Blue Dyes on an Ashitaba Waste and a Walnut Shell-Based Activated Carbon from Aqueous Solutions: Experiments, Characterization and Physical Interpretations. *Chem. Eng. J.* **2020**, *388*, 124263. [[CrossRef](#)]
48. Abdelrahman, E.A.; Khalil, M.M.H.; Algethami, F.K.; Khairy, M.; Abou El-Reash, Y.G.; Saad, F.A.; Shah, R.K.; Ammar, A.M. Facile Synthesis of MgO/CuO and MgO/Cu₃MgO₄ Binary Nanocomposites as Promising Adsorbents for the Disposal of Zn(II) Ions. *J. Inorg. Organomet. Polym. Mater.* **2023**, *in press*. [[CrossRef](#)]
49. Wu, X.; Wang, W.; Li, F.; Khaimanov, S.; Tsidaeva, N.; Lahoubi, M. PEG-Assisted Hydrothermal Synthesis of CoFe₂O₄ Nanoparticles with Enhanced Selective Adsorption Properties for Different Dyes. *Appl. Surf. Sci.* **2016**, *389*, 1003–1011. [[CrossRef](#)]

Disclaimer/Publisher's Note: The statements, opinions and data contained in all publications are solely those of the individual author(s) and contributor(s) and not of MDPI and/or the editor(s). MDPI and/or the editor(s) disclaim responsibility for any injury to people or property resulting from any ideas, methods, instructions or products referred to in the content.